NASA DEVELOP National Program

Jet Propulsion Laboratory
Fall 2014

Gulf Coast Ecological Forecasting

Utilizing Spaceborne and Airborne Sensors to Monitor the Health of Louisiana's Coastal Wetlands.

DEVELOP Technical Report
November 20, 2014

Gwen Miller (Project Lead)
Daniel Jensen
Jerry Heo
Alexandra Conner
Dr. Marc Simard, Jet Propulsion Laboratory (Science Advisor)

I. Abstract

Louisiana's coastline is home to widespread wetland ecosystems, including salt marshes and mangrove forests, which provide vital ecological services. These wetlands are extremely vulnerable to sea level rise due to climate change, urban development, and the relatively low elevation along Louisiana's coast. To assess the health, distribution, and vulnerability of tidal wetlands, a variety of datasets and models were investigated. This involved using a time series of Landsat 5 and 8 data from 1984 to present and National Wetlands Inventory data to perform change-detection. NASA's Uninhabited Aerial Vehicle Synthetic Aperture Radar (UAVSAR) and the Japanese Aerospace Exploration Agency's (JAXA) Advanced Land Observing Satellite (ALOS) Phased Array type L-band Synthetic Aperture Radar (PALSAR) data were also used to create estimates of biomass within wetlands along Louisiana's coastline. These data then informed the implementation and interpretation of two ecological models. First, the FORMAN Model was presented as a preliminary tool to assess the growth rate of Louisiana's mangrove ecosystems. Then, the Sea Level Affecting Marshes Model (SLAMM) and the Marsh Equilibrium Model (MEM) was applied to investigate wetland vulnerability and predict the response of all coastal wetlands in Louisiana to sea level rise. SLAMM implemented the Intergovernmental Panel on Climate Change's (IPCC) climate change projection A1B, which then allowed for the estimation of biomass loss with increasing sea level. With these data compiled and tools implemented, the overall health and vulnerability of Louisiana's coastal wetlands could be appraised to inform further research and official decision-making.

Keywords

Synthetic Aperture Radar, Sea Level Rise, Wetlands, Mangroves, Louisiana, Biomass, Landsat

II. Introduction

Coastal wetlands offer a variety of ecosystem services to local communities, including improved water quality, protection from storm surges, and habitat for wildlife. However, coastal wetlands in Louisiana are continually threatened by development, pollution, and rising sea levels. This is especially prevalent in Louisiana, where coastal mangroves and salt marshes have been encroached upon and degraded. To address this, the Coastal Wetlands Planning, Protection and Restoration act (Public Law 101-646, Title III CWPPRA) provides funding to help restore wetlands within Louisiana. To date over 110,000 acres of wetlands in Louisiana have benefitted from this legislation. There is limited remotely sensed data on coastal wetlands within Louisiana that have been analyzed and most projects are small-scale field measurements pertaining to biomass, salinity, nutrients and erosion rates. A large scale field study along the entire Louisiana coast is impractical, and therefore utilizing remote sensing techniques is crucial for a larger-scale analysis.

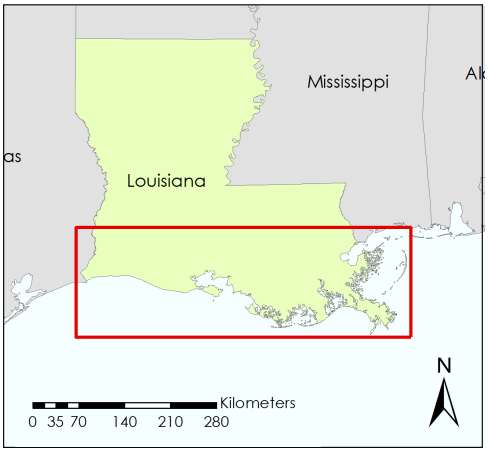

Figure 1. The project study area is within coastal Louisiana, depicted by the area within the red box.

Accordingly, this project aimed to provide analysis on the general health of coastal wetlands to understand their relationship with sea level rise and human activity, and to provide a

methodology for assessing the similar concerns in other coastal wetlands using similar data and modelling. For this ecological forecasting study, this project investigated the coast of Louisiana along the Gulf of Mexico, as seen in Figure 1, and the utilized data range in collection date from the year 1983 to 2014. In turn, modeled projections extend from the present to the year 2100. By partnering with Dr. Victor Rivera Monroy of Louisiana State University and Tom Doyle of the USGS National Wetlands Research Center, this project contributed analyses on wetland biomass and vegetation health, mangrove ecosystem productivity, and wetland response to sea level rise in order to address community concerns over the future of the region.

III. Methodology

Data that was gathered include: Landsat Satellite images; UAVSAR and ALOS PALSAR data; LiDAR and SRTM DEM; Bathymetry; Soil properties; tidal data; Land cover; Watershed; Salinity and nutrient availability; and a map of Wetlands.

Landsat Mosaicking

Data was gathered from USGS' GLOVIS website (http://glovis.usgs.gov/). 30x30 meter Landsat 5 Thematic Mapper and 8 Operational Land Imager scenes were gathered from between November and February of 1984-1985, 1993-1994, 2004-2005, and 2013-2014. The data was then atmospherically corrected using the open source software GRASS GIS and the method 'dos 4'. The atmospherically corrected tiles were mosaicked together to produce one image of the entire gulf coast.

Wetland Spectral Signatures

To obtain spectral signatures for each type of tidal wetland along Louisiana's coastline, a polygonal shapefile was obtained from the National Wetlands Inventory. The shapefile map was clipped to only include tidal wetlands and then 12 codes from the SLAMM model were incorporated into the data so that we could have 12 different maps of the different types of wetlands. The Landsat 5 and 8 images that were used in the Landsat mosaicking were used for this analysis, however, only 3 scenes along the coast were used. The 12 polygonal wetland maps were extracted from each NDVI and NIR scene for all four decades. A raster calculation was used on these mask extractions to obtain pixel values and counts and the data was incorporated into histograms, which show each wetland class per scene per decade.

Landsat Change Detections

Change detections were conducted while focusing on one scene on the outermost coast near the Sawdust Bend Bayou. Landsat 5 images from November 1984 and January 2010 were atmospherically corrected using the same dos 4 method and used to produce normalized vegetation difference (NDVI) composites to spatially understand vegetation healthiness. The near-infrared (NIR) bands were also used for vegetation distribution in this analysis. The NDVIs and NIR bands from 1984 were subtracted from the 2010 data to obtain spatial information of negative change, positive change, and areas of no change. To assess the accuracy of these maps, we produced two more change detection maps from images that were taken during summer months. Using Landsat 5 images from July 1987 and June 2011, the same NDVI and NIR change detections were conducted to ensure that the winter change detections were not showing difference based on seasonal winter variation or tidal influences.

Tide Variability with NDVI and NIR

To assess tidal variability with NDVI and NIR, five Landsat 8 Operational Land Imager scenes with minimal cloud cover were analyzed over the course of 2014. After the atmospheric

corrections, five NDVI composites were created and NIR bands were observed. A polygonal zonal statistic was conducted around the area of Port Fourchon and the average pixel values were obtained from areas that displayed lighter pixel values and darker pixel values. A comparison was made between the average high and low pixel values with the tide level (obtained through NOAA), observed at Port Fourchon, at the exact time of the Landsat image.

Biomass Mapping

Due to its complete coverage of Louisiana's coast and its moderate resolution, ALOS PALSAR data proved to be the most useful tool for comprehensive mapping of Louisiana's wetland biomass. Level 1.5 horizontally emitted, vertically received (HV) polarized data ranging in date from September 24, 2010, through December 13, 2010, were downloaded from the Alaska Satellite Facility's (ASF) User Remote Sensing Access Distributed Active Archive Center (URSA DAAC). The HV polarization was used due to its double-bounce characteristic, whereby the radar signal interacts with the ground and the vegetation canopy before returning to the sensor, allowing for a more accurate reading of biomass. Using the program Next ESA SAR Toolbox (NEST), a 3x3 mean speckle filtering was initially conducted on each data tile, followed by radiometric calibration and unit conversion into decibels (dB). The processed tiles were then mosaicked together using ArcGIS to cover the whole extent of Louisiana's coast, as can be seen in Figure 2**.**

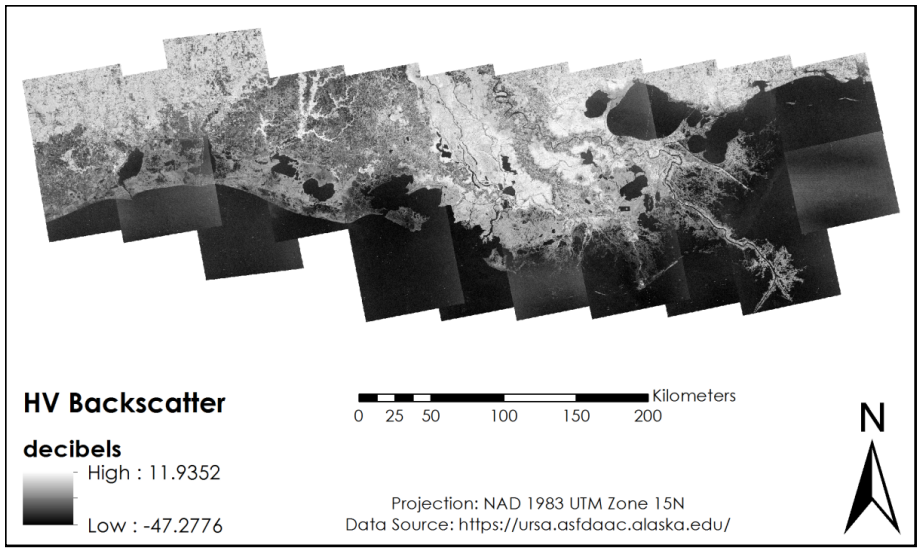

Figure 2: The mosaicked ALOS PALSAR dataset, depicting HV backscatter values (dB) for Louisiana's coastal region in late 2010.

With the ALOS PALSAR data preprocessed, the HV mosaic could be combined with biomass field data in order to build a model that enables the calculation and mapping of wetland biomass at large. The tabular biomass data, provided by Dr. Marc Simard, was imported to ArcGIS to be processed. This involved compiling the multiple overlapping points into one point to calculate the mean sampled biomass in grams per square meter at each individual coordinate pair. These points can be seen as mapped in appendix Figure A 1 . Then, the HV backscatter values underlying those points from the mosaicked data were extracted and appended to the point data so that the relationship between biomass (g/m2) and backscatter (dB) could be quantified. To this end, the table attached to the biomass point layer was exported and opened in LibreOffice Calc to perform regression analysis. Plotting the above-ground biomass values against HV backscatter for each point resulted in the graph and regression shown in appendix Figure A 2, with an R^2 of 0.515. Using ArcGIS, this model was then applied to the ALOS PALSAR data masked to the extent of the marsh types in the NWI data, thereby producing a map of above-ground biomass for Louisiana's coastal marshes.

Biomass Error Analysis

While marsh biomass was mapped using unadjusted HV backscatter data, tide level has an effect on the backscatter readings in tidally influenced ecosystems like wetlands (CITE). This necessitated accounting for tide in a separate map in order to examine the potential for error in the final biomass calculation. To do this, the tide level at the closest National Oceanic and Atmospheric Administration (NOAA) tide gauge for each ALOS PALSAR tile was examined at the time of capture through NOAA's tides and currents map (http://tidesandcurrents.noaa.gov/map/). Those values were recorded for each tile, as can be seen in Figure A 3, for adjustment. Before adjusting each tile, though, a time series of ten images for the tile containing the Port Fourchon tide gauge (tile 21) was downloaded in order to model HV backscatter's relationship with tide. A sample area corresponding to marshland around the tide gauge was drawn in ArcGIS and the average HV backscatter value in that region was recorded for each different image. Those values and their corresponding tide values were logged in LibreOffice Calc and the regression model shown in Figure A 4 was developed accordingly. The derivative of this model, then, was used to adjust each individual tile and create a new mosaic by implementing the equation below.

After this adjustment, the biomass field data points were again used to extract HV backscatter values, but this time using the mosaicked dataset that was adjusted for tide. The biomass values and adjusted backscatter values were imported into LibreOffice Calc to create the scatterplot and regression model in Figure A 5. The adjusted mosaic was then masked to the marshes' extent and this model was applied to estimate biomass with regard to tide level. With this raster dataset calculated, it was subtracted from the original biomass raster to quantify and represent potential error in the original calculation due to tide.

Difference Mapping

UAVSAR data was gathered from the Alaska Satellite Facility website as GRD files and incidence angle files in INC format. An adjacent UAVSAR strip was used to test the values after the radiometric correction and dB calculations. A Python script, provided by the project mentor Dr. Marc Simard, was used to create an HDR file for the polarized images in GRD format to be opened and processed in QGIS. A header file was also created for the incidence angle INC files to be opened in QGIS. Once both files were opened in QGIS, an equation to radiometrically correct the data, was used. The equation was the polarized image multiplied by the tangent of the incidence angle file ("polarized image" x tan("incidence angle")). Then the output image's units had to be converted to decibels(dB). To convert the values to dB, another equation (10*log10("corrected image"))was applied. The overlapping areas of the images were compared and contrasted to see if the

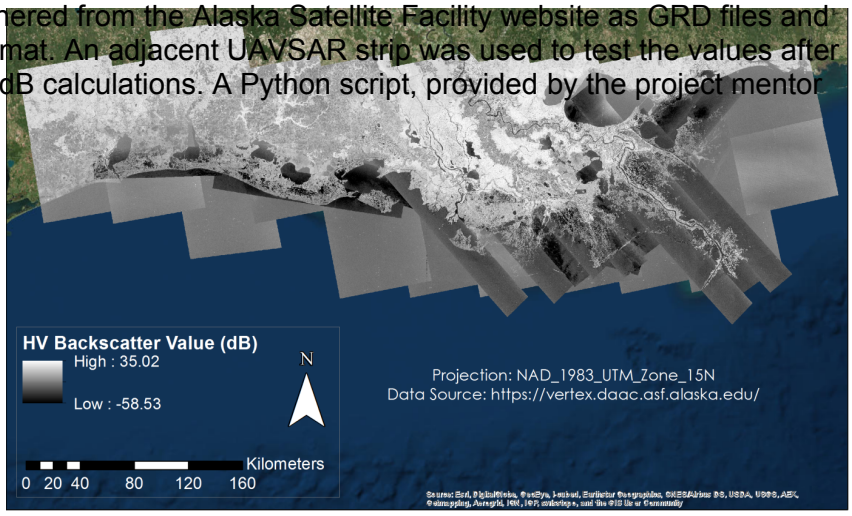

Figure 3: Final SAR mosaic of UAVSAR and ALOS PALSAR datasets after preprocessing and resampling.

resultant values were feasible. Once feasible, more flight swaths were gathered to create a large mosaic of the entire Louisiana coast, through ArcMap.

This mosaic was then further patched with the ALOS PALSAR dataset to provide a higher resolution mosaic of the study region. An already created ALOS PALSAR mosaic was first resampled to match the resolution of the UAVSAR dataset which was then mosaicked together to create one large HV polarized image of the entire Louisiana coast. This larger mosaic was created because of holes within the higher resolution UAVSAR images (Figure 3).

Since the SAR datasets vary in time of image acquisition, we conducted a difference map to use the backscatter data as a basis of wetland change. The ALOS PALSAR mosaic was taken from the year 2010 while the majority of the UAVSAR dataset was from 2014. The UAVSAR data was subtracted by the ALOS PALSAR data ("ALOS PALSAR" – "UAVSAR") to output this difference map which provides information of change in wetland extent.

Forman model

LiDAR DEM was gathered from the Louisiana State University Virtual Coast Data Archive and the newest SRTM DEM data was taken from JPL's website. Both DEMs were first mosaicked then incorporated in an equation using the raster calculator in ArcGIS to output a canopy height map. In 1989 there was a freeze that killed most of the mangroves within Louisiana, and the SRTM DEM was acquired in 2000. This allowed us to estimate mangrove growth rate based on an eleven year time period. We were able to estimate nutrient availability using salinity, light availability, growth rate and a DEM by working backwards within the Forman model.

The Forman model was used to calculate growth potential in accordance with the Chen and Twilley's (1998) study:

where, G is a growth constant for a specific mangrove species, D is the tree trunk diameter at breast height (cm), H is tree height (cm), S(SALT) is the salinity multiplier, N(Nut) is the nutrient multiplier, T(DEGD) is the temperature multiplier, and r(AL) is relative light availability. Growth potential is a measurement of diameter at breast height growth for a given species and is directly affected by the four environmental multipliers. The model used parameters fitted for *Avicennia germinans* for growth potential because it is the only species of mangroves in Louisiana. The salinity raster was acquired by taking salinity values from gauges and interpolating the data to create a continuous raster. Both USGS and Louisiana Department of Environmental Quality gauges were used to obtain salinity readings. Growing degree days were obtained from the Integrated Plant Protection Center of Oregon State University's US degree-day mapping calculator (http://pnwpest.org/cgi-bin/usmapmaker.pl). Available light was a constant found within Chen and Twilley's (1998) study. We used Python to write the model code and used gdal, rasterio and numpy to run calculations on the rasters. Python was used to allow our model to be open sourced.

Sea Level Rise Affecting Marsh Model (SLAMM)

SLAMM is a downloadable software that needs at least three input ascii files, DEM, SLAMM categories and slope. This model is a physical model, as opposed to biological model, that is used to predict how wetland type with change overtime. We used a 30 meter resolution SRTM DEM, ArcGIS to derive slope from the DEM, and used a National Wetlands Inventory raster that was categorized into SLAMM wetland categories. We chose the IPCC A1B sea level rise scenario within the tool and modeled wetland change for every 25 years until year 2100.

Marsh Equilibrium Model (MEM)

MEM is used to estimate both productivity and elevation change within marsh ecosystems. The model uses both elevation as well as biological inputs. We used python to write the MEM model and used gdal, rasterio and numpy within the script to perform raster calculations. Change in marsh productivity and marsh elevation was derived from the following equations developed by Morris et al. (2002)

where B is productivity ($g*m^{-2}*yr^{-1}$) a, b and c are model coefficients, dY_2/dt is change in marsh elevation (cm), D is depth (cm), q is sediment loading, k is trapping efficiency. To find depth we subtracted the LiDAR DEM from a mean higher high sea level raster. Negative values were set to zero since this indicates that the area is above sea level at higher high tide and thus there is no depth. Values for coefficients a, b, and c were the same as those within Morris et al. (2002). Using our produced marsh biomass raster we determined regions of high and low biomass. We set regions with high biomass to have a sediment loading of 0.0018 and low biomass to be 0.00018 and trapping efficiency was set to 0.000015. These values were obtained from Morris et al. for regions with high or low sediment trapping efficiencies (2002).

IV. Results & Discussion

Wetland Spectral Signature Analysis

The histograms that were created to analyze wetland type and pixel values and counts did not provide clear enough distinctions for spectral signature conclusions. We cannot conclude that wetlands types are distinguishable by NDVI or NIR in this scenario. The individual histograms show wetland types having very similar spectral signatures. However, the wetland types vary immensely from decade to decade and from scene to scene. The wetland types lie between 0.2 and 0.5 pixel values for NDVI and between 0 and 0.3 pixel values for NIR data (Figure 5).

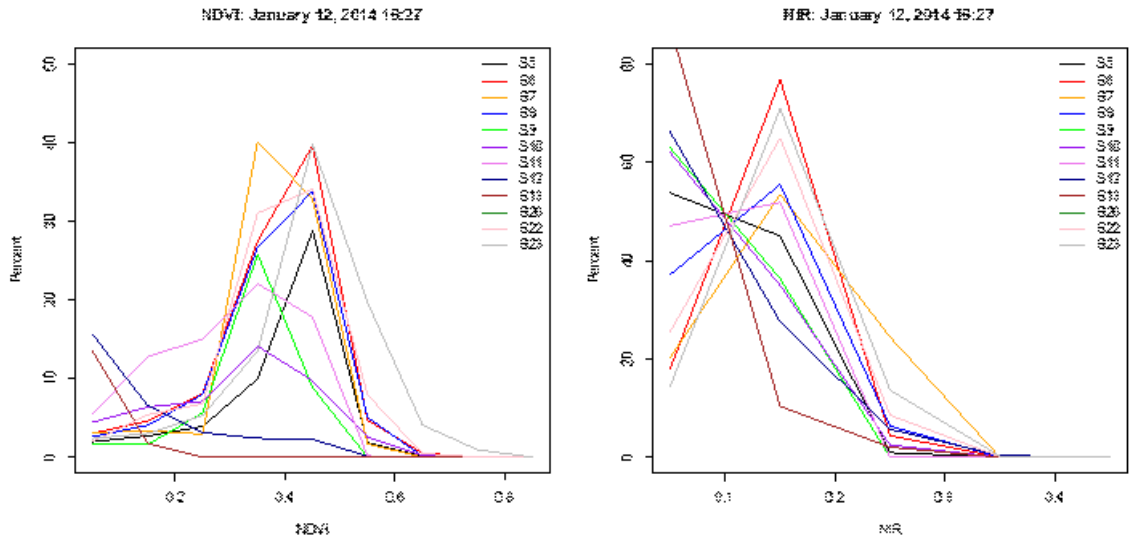

Figure 5: Histograms showing pixel values and counts of wetland types of 2014 NDVI and NIR.

Change Detection Analysis

The NDVI and NIR change detections between summer and winter were strongly comparable. The NIR change detection proved 48.1% negative change in the winter and 64.2% in the summer, 50.9% positive change in the winter and 34.4% in the summer, and approximately 0.8% no change in the winter and 1.3% in the summer. The NDVI change detection shows 67.7% negative change in the winter and 67.4% in the summer, 31.9% positive change in the winter and 32.3% in the summer, and 0.2% no change in the winter and 0.3% in the summer. The summer and winter NDVI numbers are far more similar than those of the NIR. Although the percentages vary from NDVI and NIR and there are seasonal variations between summer and winter, there is a clear spatial similarity of the vegetation/wetland losses and gains. All four maps show a distinct negative change in around the Garden Island Bay area and positive change east of the Mississippi River near the Willow Bauyou and we are confident in the loss and gain shown in this areas.

Tide Variability Analysis

NDVI and NIR images will be influenced by greenness, atmospheric corrections, and tide. However, in this scenario, we assessed that there is not necessarily variability of NDVI and NIR with tide because there is seemingly no correlation between high NDVI and NIR and low tide (and low NDVI/NIR and high tide; Figure 6). The weak correlation could be influenced by cloud cover, which could provide erroneous NDVI and NIR pixel values, even after the images have been atmospherically corrected. Another area and port should be analyzed with the same methods.

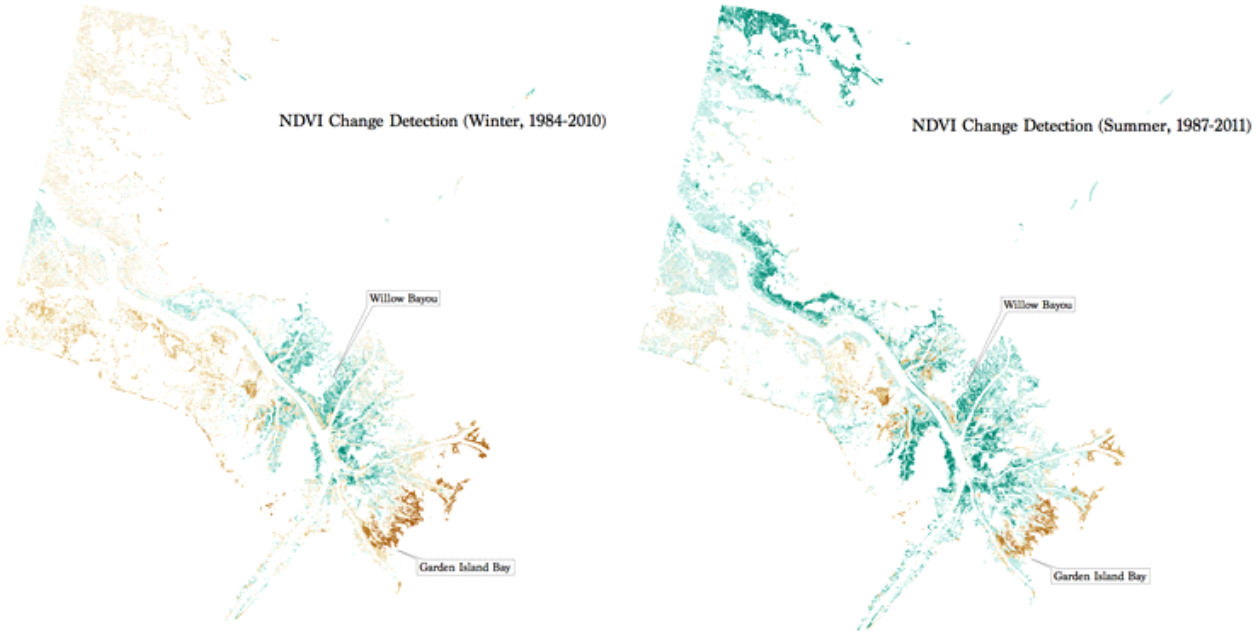

Figure 6: Maps of change detection of winter 1984 and 2010 NDVI and summer of 1987 and 2011 NDVI. Both figures show brown as negative change and blue as positive change.

Biomass Analysis

Louisiana's marshes contain regions that are severely degraded with very little vegetation biomass (Figure 7). In particular, the marsh region around Port Fourchon, to the west

of the Mississippi River delta shows widespread low-biomass, indicating severe degradation. Other areas of concern that show severely low biomass include Marsh Island west of that region, the nearby shore west of Marsh Island, and the wetlands fringing Louisiana's northeast shore.

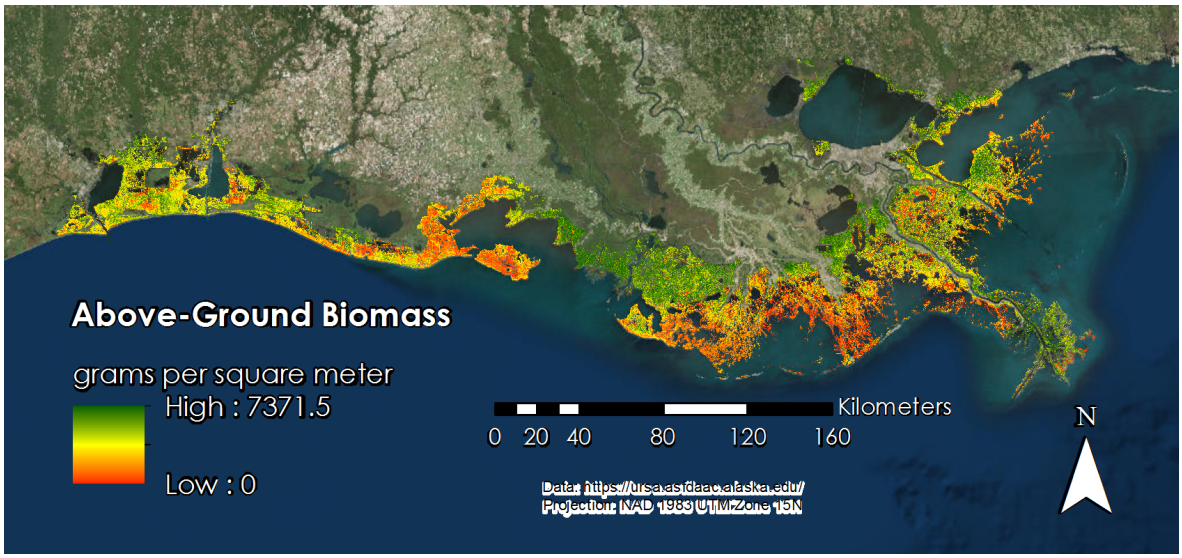

Figure 7: A biomass map of Louisiana's marshes, in grams per square meter. This map product was derived from ALOS PALSAR and National Wetlands Inventory data.

This map and the underlying data is a good preliminary indicator of marsh biomass, but there are several confounding factors that must be noted. The first such factor is the limitation inherent in the biomass field data. The utilized dataset contained only nineteen individual biomass sample plots within Louisiana's marshland, which is a limited number of data points with which to build a regression model. Furthermore, the geolocated coordinate pairs attached to those points have uncertain accuracy, so their mapped location may be slightly shifted from their actual location. Nonetheless, the regression model built from those points still shows a clear relationship with an R^2 of 0.515 and a visually distinct linear relationship through the majority of the points. With regards to the biomass field data's shortcomings, then, a more comprehensive dataset with more sample sites would enable a more accurate model with a theoretically higher R^2 to be developed. Despite this, the results of the biomass calculation in Figure # appear to be sound based on its correlation with both the Landsat and HV backscatter difference analyses in **Figures # and #.**

Another factor that introduces error potential into the above-ground biomass results is tide. Local tide has an appreciable effect on SAR backscatter readings in tidal wetlands, as higher water levels amongst vegetated areas lower the backscatter value, and vice versa. As such, quantifying the mapped biomass data's potential for error based on tide is an important aspect of interpreting those results. This analysis produced a second biomass map which is based on the PALSAR data corrected for local tide levels (Appendix Figure A 6). As that map shows, there are regions that are visually distinct along the tiles' borders. This is due to those regions having an extremely high tide relative to the rest of the regions. Equivalent tide values were not available or represented in the backscatter versus tide model, so those regions with extreme values tides in the original data contain the most potential for error. With this in mind, the error potential map in Figure 9 was calculated by subtracting the tidally adjusted biomass raster from the regular biomass raster. As **Figure #** shows, there is greater uncertainty in those regions with more extreme tide levels at the time ALOS captured the utilized data. Higher error

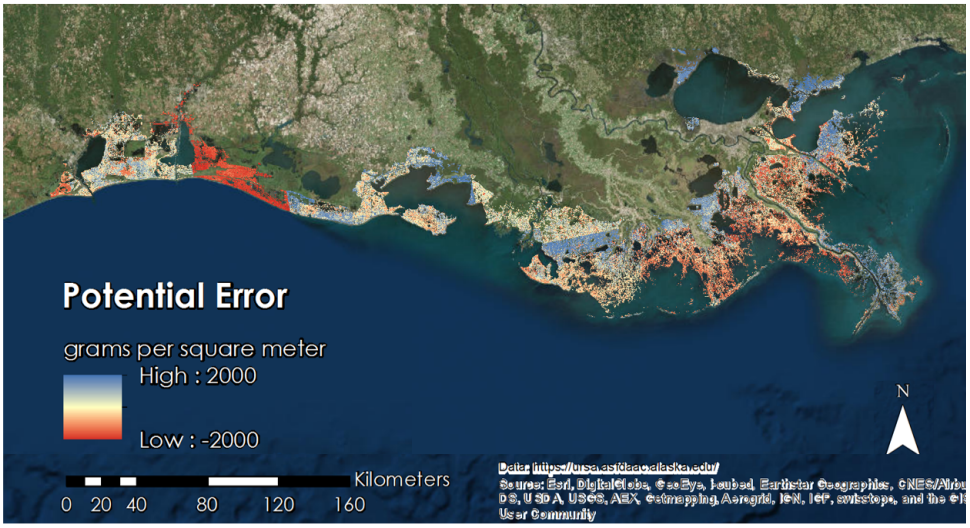

Figure 9: Error potential calculated derived from the tidally adjusted biomass and regular biomass rasters. These values indicate how far each pixel may have been overestimated or underestimated in the original biomass calculation based on tidal influence.

potential is denoted by the deep red and blue colors, and the map shows that the areas with

significant areas are largely regions with medium to high biomass estimates. However, the aforementioned regions of interest that are subject to degradation and severely low biomass are largely areas with middling error potential. This affirms the conclusion presented by the biomass calculation that those areas indeed show abnormally low biomass values that cannot be attributed purely to error. With this methodology, analysis, and set of maps in place, it is clear that biomass mapping using L-band radar is an effective tool for assessing wetland health.

Difference Map

The difference map shows the changes in backscatter values in decibels (dB) from the ALOS PALSAR and UAVSAR mosaics. The backscatter values could then be interpreted as overall biomass change depending on the high and low values that is depicted. In Figure 10 high values represent marsh wetland loss, while the low values represent gain. There is a

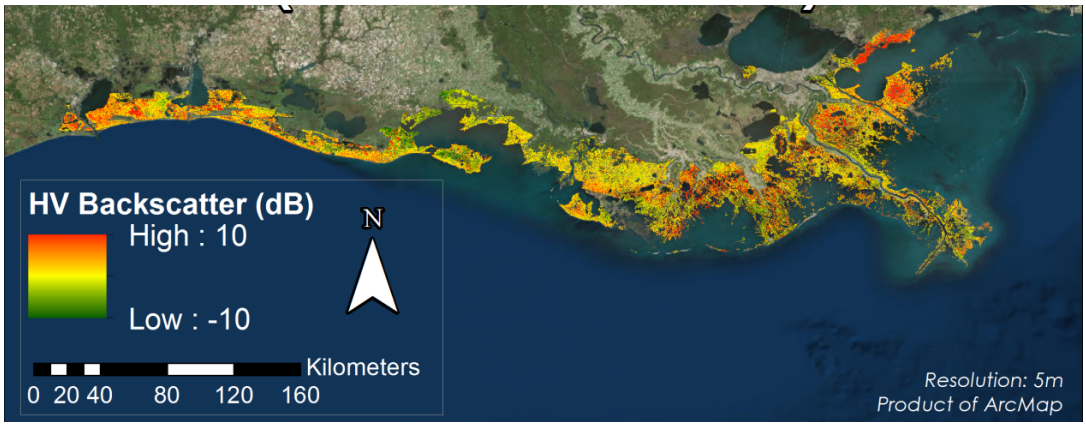

Figure 10: A difference map between ALOS PALSAR and UAVSAR mosaics to portray change in HV backscatter values. The images from ALOS PALSAR were acquired in 2010, and in 2014 for the majority of the UAVSAR mosaic. High (red) values correlate with areas of marsh wetland loss and low(green) values with marsh wetland gain. This can be used for decision making purposes through biomass change detection, highlighting degraded areas.

correlation between the areas of wetland loss and gain with the amount of biomass estimated using ALOS PALSAR images, providing possible applicability of radar backscatter data. The data correlates well when also comparing the NDVI change detection maps.

Sea Level affecting Marsh Model (SLAMM)

The Sea Level Rise affecting Marsh model shows that marshes are retreating upland (Figure 11). There is also a large amount of marsh wetland loss from present day to year 2025 which will result in significant biomass loss (roughly 2358000 metric tons). This reduction in biomass within marshes will likely contribute to an overall reduction in carbon storage. If carbon storage is not increased

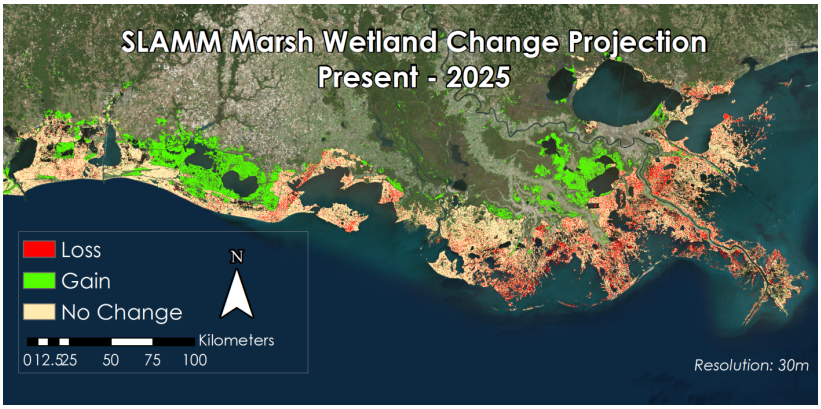

Figure 11. Modeled marsh wetland change from present day to year 2025 using SLAMM and the A1B sea level rise scenario.

elsewhere, this will decrease the capacity of Louisiana's marshes to help combat climate change.

Forman Model

Mangrove extent within Louisiana is sparse and mangrove height is relatively small in comparison with other mangrove groves. Mean mangrove height within Louisiana is roughly two meters, and the diameter at breast height growth rate vary from 0.002 cm/yr to 0.9 cm/yr (Figure 11). There is no inherent observable pattern to differences in growth rates due to the diffuse mangrove strands. Further analysis should be conducted to better understand the key drives in mangrove growth rates.

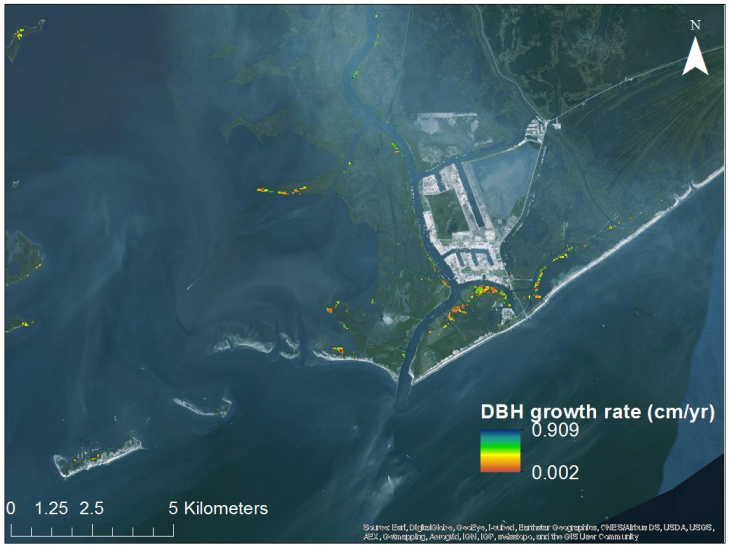

Figure 12. Diameter at breast height (DBH) growth rate (cm/yr) for mangroves within Port Fourchon.

Marsh Equilibrium Model (MEM)

Within MEM we successfully estimated change in marsh elevation and estimated above ground productivity (Figure 13). Comparing the estimated change in elevation over one year to estimated sea level rise in combination with land subsidence we were able to determine if marsh elevation change can keep up with sea level rise. The outputs of MEM suggests that a large area of marshes will become submerged (Figure 14). To improve accuracy of the model field research should be conducted to better estimate sediment trapping efficiency.

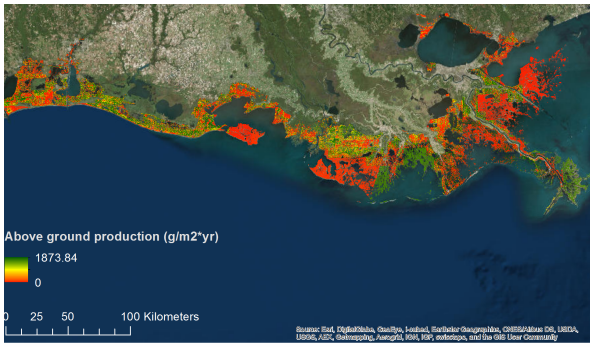

Figure 13: Modeled above ground biomass for marshes within Louisiana's coast.

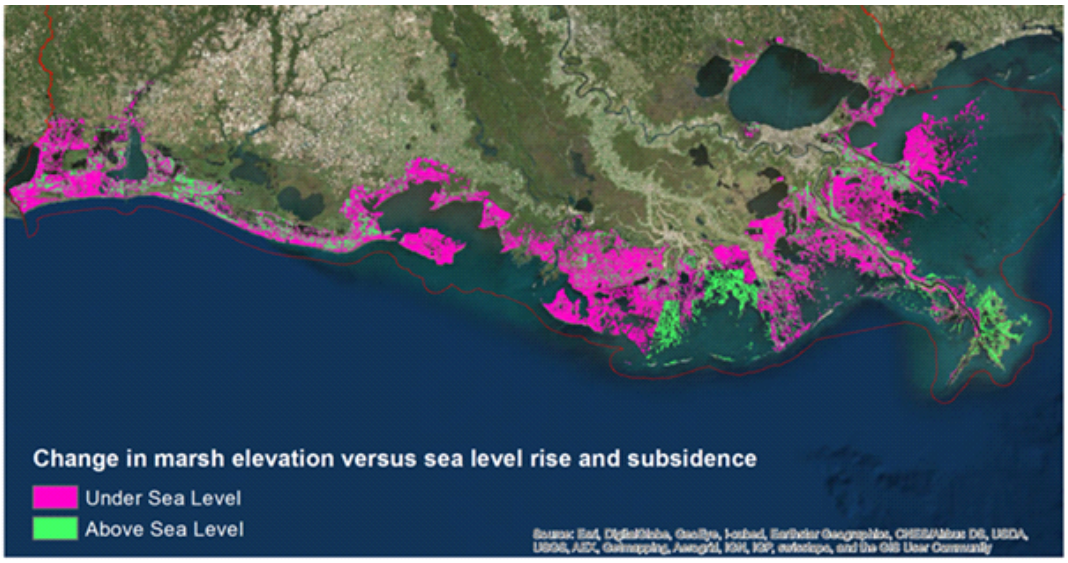

Figure 14: Change in marsh elevation over one year versus rise in sea level over one year. Areas in green are regions where marsh elevation is projected to change at the same rate or faster than sea level rise and subsidence. Sea level rise and subsidence is estimates at 9mm/yr.

V. Conclusions

The biomass mapping methods proved to be fairly robust in providing estimates of wetlands in the Louisiana coast. With an R^2 of 0.52 on the regression model, biomass maps helped us visualize the extent of wetland gain and loss. Biomass estimation was also estimated for the UAVSAR dataset, but ended in low correlations with the backscatter values due to poor biomass point coordinates. However, these maps can be bolstered with more comprehensive biomass field data. A difference map between the SAR datasets proved to be useful in showing similar marsh wetland change. Using the SLAMM model, wetland marsh response to sea level rise was estimated for the years 2025, 2050, 2075, and 2100. An estimated 10,708,588 metric tons, of existing marsh biomass, are projected to be lost by 2100 due to sea level rise. The change detection analyses of NDVI and NIR proved to be effective tools to map wetland extent and vegetation loss and gain, but lacked correlations with tidal fluctuations and could have easily been influenced by atmospheric disturbances in the data. Conducting such large scale analyses with remote sensing tactics, we were able to assess a gradual marsh wetland decline in Louisiana's coastline.

VI. Acknowledgments

We would like to thank our science advisor, Dr. Marc Simard for his work and guidance on this project. We would also like to thank Scott Baron for his contributions on the previous phase of this project, especially for his work scripting the Forman model. Lastly, we would like thank our project partners for their advice and contributions.

VII. References

About CWPPRA. Not Dated. *Louisiana Coastal Wetlands Planning Protection and Restoration Act Program*. http://lacoast.gov/new/About/.
Chen, R., and R. R. Twilley. 1998. A gap dynamic model of mangrove forest development along gradients of soil salinity and nutrient resources. *Journal of Ecology* 86 (1):37–51.
Day, J. W., A. Y. Arancibia, W. J. Mitsch, A. L. Lara-Dominguez, J. N. Day, J.-Y. Ko, R. Lane, J. Lindsey, and D. Z. Lomeli. 2003. Using Ecotechnology to address water quality and wetland habitat loss problems in the Mississippi basin: a hierarchical approach. *Biotechnology Advances* 22 (1-2):135–159.
Giri, C., J. Long, and L. Tieszen. 2011. Mapping and Monitoring Louisiana's Mangroves in the Aftermath of the 2010 Gulf of Mexico Oil Spill. *Journal of Coastal Research* 277 (6):1059–1064.
Hamdan, O., H. Khali Aziz, and I. Mohd Hasmadi. 2014. L-band ALOS PALSAR for biomass estimation of Matang Mangroves, Malaysia. *Remote Sensing of Environment* 155:69–78.
Morton, R., J. Bernier, and J. Barras. 2006. Evidence of regional subsidence and associated interior wetland loss induced by hydrocarbon production, Gulf Coast region, USA. *Environmental Geology* 50 (2):261–274.
Mougin, E., C. Proisy, G. Marty, F. Fromard, H. Puig, J. L. Betoulle, and J. P. Rudant. 1999. Multifrequency and multipolarization radar backscattering from mangrove forests. *IEEE Transactions on Geoscience and Remote Sensing* 37 (1):94–102.
Rivera-Monroy, V. H., R. R. Twilley, S. E. Davis, D. L. Childers, M. Simard, R. Chambers, R. Jaffe, J. N. Boyer, D. T. Rudnick, K. Zhang, E. Castañeda-Moya, S. M. L. Ewe, R. M. Price, C. Coronado-Molina, M. Ross, T. J. Smith, B. Michot, E. Meselhe, W. Nuttle, T. G. Troxler, and G. B. Noe. 2011. The Role of the Everglades Mangrove Ecotone Region (EMER) in Regulating Nutrient Cycling and Wetland Productivity in South Florida. *Critical Reviews in Environmental Science and Technology* 41 (1):633–669.
Simard, M., K. Zhang, V. H. Rivera-Monroy, M. S. Ross, P. L. Ruiz, E. Castañeda-Moya, R. R. Twilley, and E. Rodriguez. 2006. Mapping Height and Biomass of Mangrove Forests in Everglades National Park with SRTM Elevation Data. *Photogrammetric Engineering & Remote Sensing* 72 (3):299–311.

VX. Appendix A

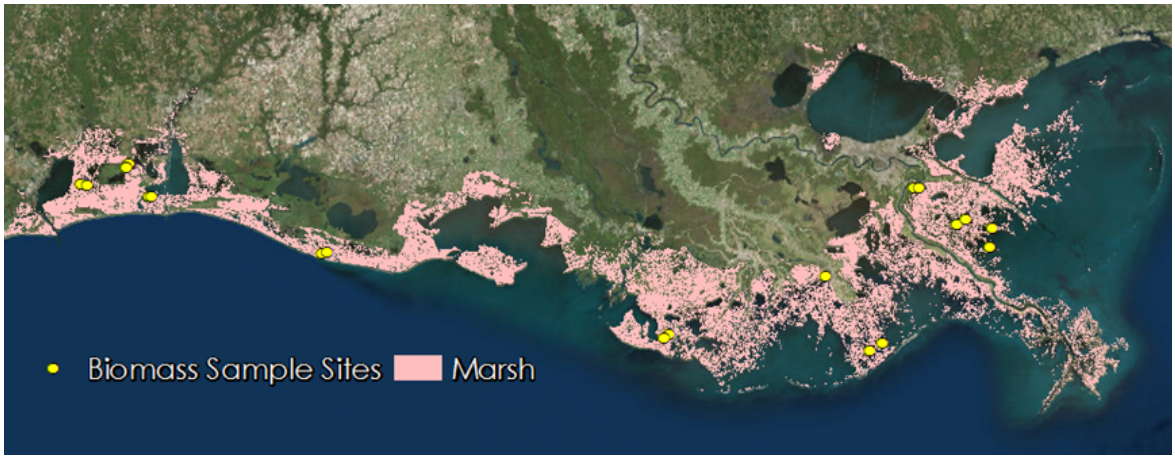

Figure A 1: The location of the biomass sample sites overlaid on the extent of marshes from the National Wetlands Inventory.

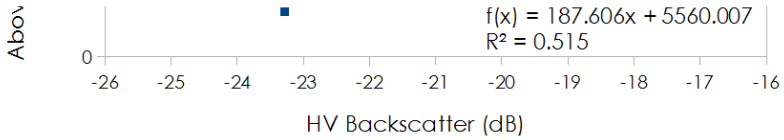

Figure A 2: The scatterplot and regression model derived from the ALOS PALSAR HV data and the biomass field data. The regression model was used to calculate marsh biomass.

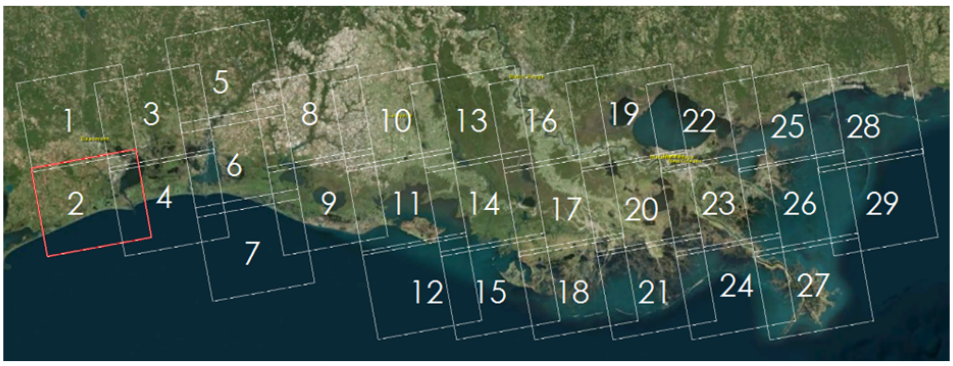

Tile #	Date	Time	Tide Level (m)	Closest Station		Date	Time	Tide Level (m)	Closest Station
1	12/1/2010	4:46:24	-0.401	Port Arthur (TCOON), TX	15	12/8/2010	4:35:16	0.016	LAWMA, Amerada Pass, LA
2	12/1/2010	4:46:15	-0.325	Sabine Pass North, TX	16	11/21/2010	4:33:42	-0.213	Berwick, LA
3	11/14/2010	4:44:34	-0.131	Port Arthur (TCOON), TX	17	11/21/2010	4:33:34	-0.213	Berwick, LA
4	11/14/2010	4:44:26	0.062	Sabine Pass North, TX	18	11/21/2010	4:33:25	0.276	LAWMA, Amerada Pass, LA
5	12/13/2010	4:42:02	-0.819	Bulk Terminal, LA	19	11/4/2010	4:31:51	0.269	New Canal Station, LA
6	12/13/2010	4:41:53	-0.819	Bulk Terminal, LA	20	11/4/2010	4:31:42	0.056	West Bank 1, Bayou Gauche, LA
7	12/13/2010	4:41:45	-0.845	Calcasieu Pass, LA	21	11/4/2010	4:31:34	0.155	Port Fourchon, LA
8	11/26/2010	4:40:02	0.446	Freshwater Canal Locks, LA	22	12/3/2010	4:29:12	-0.206	New Canal Station, LA
9	11/26/2010	4:39:54	0.369	Freshwater Canal Locks, LA	23	12/3/2010	4:29:04	-0.17	West Bank 1, Bayou Gauche, LA
10	9/24/2010	4:38:53	0.392	Freshwater Canal Locks, LA	24	12/3/2010	4:28:55	-0.039	Grand Isle, LA
11	9/24/2010	4:38:45	0.392	Freshwater Canal Locks, LA	25	11/16/2010	4:27:21	0.457	Bay Waveland Yacht Club, MS
12	9/24/2010	4:38:37	0.392	Freshwater Canal Locks, LA	26	11/16/2010	4:27:13	0.119	Shell Beach, LA
13	12/8/2010	4:35:33	-0.314	Berwick, LA	27	11/16/2010	4:27:05	0.173	Pilots Station East, SW Pass, LA
14	12/8/2010	4:35:24	-0.314	Berwick, LA	28	10/30/2010	4:25:28	0.056	Pascagoula NOAA Lab, MS
					29	10/30/2010	4:25:20	0.056	Pascagoula NOAA Lab, MS

Figure A 3: The footprints of each tile in the mosaicked ALOS PALSAR dataset and its corresponding date, time, tide level, and closest NOAA tide gauge.

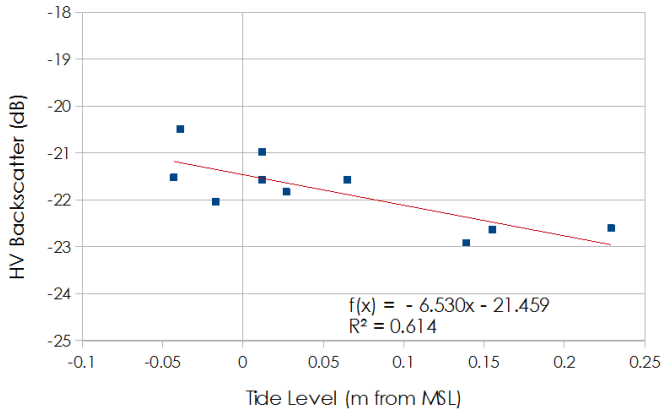

Figure A 4: The scatterplot and regression model derived from the ALOS PALSAR HV data (decibels) and tide level (meters from mean sea level) at NOAA's Port Fourchon tide gauge.

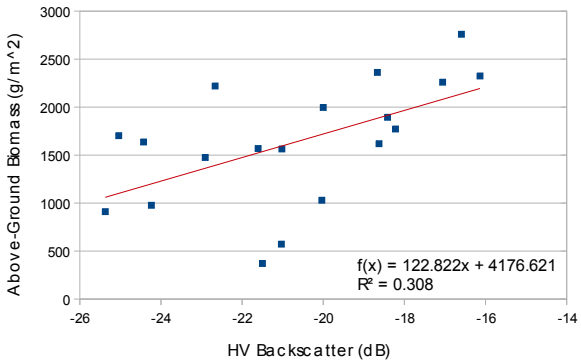

Figure A 5: The scatterplot and regression model derived from the ALOS PALSAR HV data adjusted for tide and the biomass field data. The regression model was used to estimate potential error due to tide level in the previous biomass calculation.

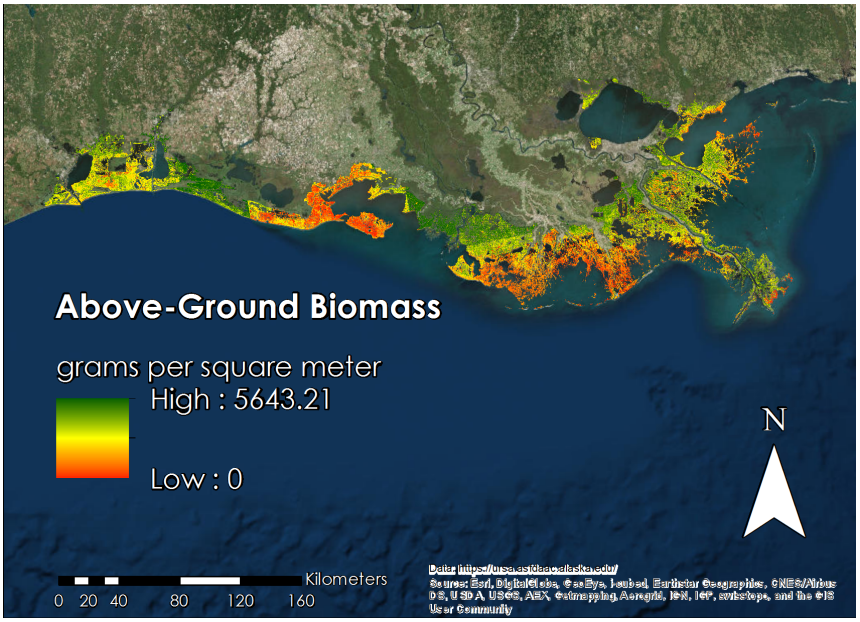

Figure A 6: Louisiana marsh biomass derived from tidally-adjusted ALOS PALSAR data.

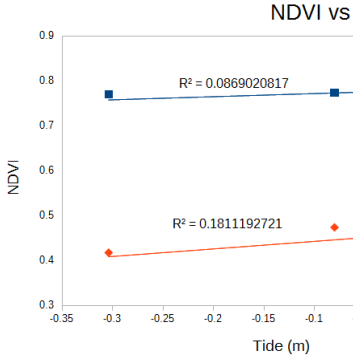

Figure A 7: Graph of high and l
at the time of each image.